

Control and imaging of molecular quantum states with second-scale coherence

Yan Zhou^{1*}, Yuval Shagam^{1*}, William B. Cairncross¹, Kia Boon Ng¹, Tanya S. Roussy¹, Tanner Grogan¹, Kevin Boyce¹, Antonio Vigil¹, Madeline Pettine¹, Tanya Zelevinsky², Jun Ye¹, Eric A. Cornell¹

¹*JILA, NIST and University of Colorado, and Department of Physics, University of Colorado, Boulder CO 80309-0440, USA*

²*Department of Physics, Columbia University, New York, NY 10027-5255, USA*

Cold molecules provide a platform for a variety of scientific applications such as quantum computation¹, simulation², cold chemistry³, and searches for physics beyond the Standard Model⁴. Mastering quantum state control and measurement of diverse molecular species is critical for enabling these applications. However, state control and readout are difficult for the majority of molecular species due to the lack of optical cycling transitions. Here we demonstrate internal state cooling and orientation-selective photofragment imaging in a spin precession measurement with multi-second coherence, allowing us to achieve the quantum projection noise (QPN) limit in a large ensemble of trapped molecular ions. We realize this scheme for both HfF^+ and ThF^+ — molecules chosen for their sensitivity to beyond Standard Model physics rather than their amenability to state control and readout.

A wide range of quantum science over the past decade has been enabled by manipulation

*These authors contributed equally to this work.

of molecules at the level of single or few quantum states⁵⁻¹⁴. Controlling external and internal molecular degrees of freedom to a single quantum state has been shown to turn chemical reactions on and off⁷ and has enabled the observation of quantum degeneracy in molecules¹⁵. Utilizing long-range dipolar interactions, molecular control can also be leveraged for quantum simulations and computation¹⁶⁻¹⁸. In addition, specific molecular structures can provide enhanced sensitivity to new physics beyond the Standard Model^{13,19-22}.

The high multiplicity of closely spaced levels in molecules means that any desired coherent signal may be highly diluted, as hundreds of thermally populated irrelevant levels will contribute nothing but background noise. For large ensembles of neutral or ionic molecules specifically chosen for their relatively simple structure and highly diagonal Franck-Condon factors (FCFs), optical pumping has been used to cool internal and external degrees of freedom^{9-12,23,24}. For experiments with single molecular ions, quantum logic spectroscopy (QLS) is a *state-of-the-art* method that has high efficiency and fidelity for both state preparation and detection^{5,6}. However, although a proposal exists²⁵, QLS has not been demonstrated in a system with multiple ions. By introducing broadband microwave couplings^{9,26} we extend the benefits of optical pumping to less pliable molecules, HfF^+ and ThF^+ , which are chosen instead for their utility in a laboratory particle physics experiment^{19,27}.

To fully harvest the benefit of a high count rate one must suppress the noise down to the QPN limit. However, the most broadly applicable methods for state-sensitive molecular detection often involve action spectroscopy, e.g. photoionization or photodissociation, and these methods are

frequently contaminated with noise well in excess of QPN. In these methods, laser fluctuations give rise to excess noise on the detected ion number, N , with standard deviation αN , while QPN scales as $N^{1/2}$. For instance, our experimental cycle of molecule creation, preparation, and detection involves five pulsed lasers, four of which are frequency doubled. Even with careful monitoring of laser frequencies and intensities, we observe shot-to-shot technical noise in excess of $\alpha = 0.2$. We have circumvented this limitation by implementing orientation-selective photofragment imaging, which allows us to count the ion populations in two distinct molecular orientations in a single cycle. Using the inherent correlation between these two populations that are prepared and read out by the same laser pulses, we are able to make differential measurements at the QPN limit while detecting hundreds of ions in each cycle.

Most quantum science studies with molecules begin with the preparation of the ensemble in a well-defined quantum state. However, this is not straightforward for the majority of molecular species. For example, we create ThF^+ in four rotational states of the ground vibronic state, $^3\Delta_1$, $v = 0$, by resonance enhanced multiphoton ionization (REMPI)²⁸. Counting the hyperfine, Zeeman, and Ω -doublet sublevels, about 100 states are populated. To concentrate the population into a single quantum state, we leverage the ideas developed for laser cooling molecules with some modifications²⁶ to compensate for highly off-diagonal FCFs. Lessons from laser cooling neutral molecules include²⁹: (1) the necessity of $\Delta J = -1$ in all optical transitions to enforce rotational cooling, (2) using fields such as microwaves to mix ground rotational states, which reduces the required number of lasers, and (3) employing vibrational repump lasers to recover population lost to excited vibrational states. While the photon scattering rate of molecules is usually low, especially

with the addition of microwave couplings, we enjoy considerable time to perform our cooling because our molecular ions are trapped. Since we are only cooling internal degrees of freedom starting with a few initial rotational states resulting from REMPI, scattering a few photons is sufficient versus $\sim 10^5$ photons as in most molecular cooling experiments.

In our ThF^+ experiment, we employ these ideas to optically pump the majority of the population to the $^3\Delta_1$, $v = 0$, $J = 1$, $m_F = \pm 3/2$ stretched states, where v , J , and m_F represent the quantum numbers of the vibration, rotation, and total angular momentum projection onto the rotating electric bias field that polarizes the molecules³⁰, respectively. We begin by rotationally cooling molecules via optical transitions to the $\Omega = 0^-$ electronic state, which forms a nearly closed system with $^3\Delta_1$ for electronic transitions (Fig. 1(a)). We drive the $J = 2 \rightarrow J' = 1$ transition to enforce rotational closure, and use microwave couplings to cool molecules in higher rotational states (Fig. 1(b)). We transfer 85% of the population to $^3\Delta_1$, $v = 0$, $J = 1$ state after 20 ms with additional $v = 1$ vibrational repumping (Fig. 2).

We prepare spin-polarized stretched states, $|m_F = 3/2, \Omega = \pm 1\rangle$, via the application of circularly polarized light as shown in Fig. 1(c). The quantum number Ω denotes the projection of J onto the internuclear axis. We accumulate 60% of the total population in the stretched states after 40 ms (Fig. 2), which are the initial states in our spin precession measurements. We further prepare a single stretched state with a specific molecular orientation (given by $m_F\Omega$), such as $|m_F = +3/2, \Omega = +1\rangle$, by applying a microwave field to resonantly depopulate the unwanted stretched state to $^3\Delta_1$, $J = 2$, where it is immediately recycled via the optical transition to $\Omega = 0^-$,

$J = 1$. Overall, we transfer 50% of trapped molecules to the target state after 50 ms (Fig. 2).

High-fidelity, low-noise quantum state readout is as critical as state preparation for studies with an ensemble of molecules. We have previously demonstrated high-yield signal readout by resonance-enhanced multi-photon dissociation (REMPD), followed by mass spectrometry to distinguish the Hf^+/Th^+ photodissociation products from background $\text{HfF}^+/\text{ThF}^+$, refs. (31, 32). In this work, enabled by our quantum state control, we incorporate photofragment-ion imaging with orientation selectivity for low-noise state readout at the QPN limit with hundreds of signal molecules. We can extract information about molecular orientation if we meet two criteria: (1) the intermediate and final states must inherit the spatial orientation of the ground state, which maps the molecular orientation to momentum-space anisotropy of the photofragments; (2) the photofragments must have a large kinetic energy compared to the ensemble temperature so as to convert the momentum-space anisotropy to a spatially resolved pattern³³.

The first REMPD photon excites the molecules from the ${}^3\Delta_1, v = 0, J = 1$ state to a bound intermediate state, $|\Omega_i = J_i = M_i = 2\rangle$, maintaining the molecular orientation for $M_i \neq 0$. M is the projection of J on the electric bias field. For the stretched states, m_F and M are mapped one to one. We only use states with $|M| = |\Omega|$ for the highest orientation contrast between states with opposite orientations. The second REMPD photon couples the intermediate state to dissociating states, breaking $\text{HfF}^+/\text{ThF}^+$ ions into Hf^+/Th^+ ions and neutral F atoms, as shown in Fig. 3(a). The angular distribution of the photofragments can be determined by evaluating the transition probability between the initial and final states³⁴. Some resulting distributions are calculated and

shown in Fig. 3(b). Experimentally, we observe a mixture of final states with different kinetic energies, and possibly different values of Ω_f . More details are given in Ref. [35]. We have obtained similar orientation contrasts in both HfF⁺ and ThF⁺ experiments.

As our REMPD detection scheme uses spectrally broad pulse lasers, it suffers from large excess noise on the total ion detection — for example, $\alpha \approx 0.2$ in our HfF⁺ experiment³⁶. While for small sample size, $N \lesssim 10$, the QPN limit is reached, excess noise dominates at our typical sample size $N \gtrsim 500$. By simultaneously detecting both molecular orientations, we can perform a differential measurement that cancels all common-mode fluctuations arising from ionization, state preparation, and detection. Moreover, we can cancel the phase noise (for example arising from fluctuations in our magnetic bias field) in our spin precession measurement that is sensitive to the electron’s electric dipole moment (eEDM).

In our eEDM measurement we perform simultaneous spin precession measurements between the $m_F = \pm 3/2$ states in the upper and lower Stark doublets ($m_F \Omega = -3/2$ and $+3/2$, respectively). The eEDM signal contributes to the differential spin precession phase between these doublets. In a single experimental cycle, we simultaneously detect the populations of two states with the same m_F . In two adjacent cycles, we measure N_A and N_C followed by N_B and N_D in Fig. 3(a), which we use to compute the spin polarizations in the upper and lower Stark doublets

$$\wp_u = \frac{N_A - N_B}{N_A + N_B} \sim C \sin \phi^u \quad (1)$$

$$\wp_l = \frac{N_C - N_D}{N_C + N_D} \sim C \sin \phi^l \quad (2)$$

where C is the spin precession contrast, and ϕ^u and ϕ^l are the spin precession phases of upper

and lower doublets, respectively. Fig. 4 shows experimental measurements of the phase evolution with up to ~ 1.5 s interrogation time. A difference in the magnetic moment of the upper and lower doublet states gives rise to a beating between the spin precession fringes.

When near the zero crossing and when the spin precessions of the upper and lower doublets are in phase, $\phi^u - \phi^l \approx 2n\pi$, the phase difference is proportional to the spin polarization difference, $\Delta\varphi = \varphi_u - \varphi_l \sim C(\phi^u - \phi^l)$. The eEDM sensitivity is ultimately determined by the measurement uncertainty of this spin polarization difference ($\Delta\varphi$). If the spin precessions of the upper and lower doublets are evaluated independently, ignoring any correlations, we might anticipate the total scatter to be $(\sigma_{\varphi_u}^2 + \sigma_{\varphi_l}^2)^{1/2}$, depicted by the blue diamonds in Fig. 4, which is five times higher than the QPN limit (dotted gray line) due to excess noise in ion production and detection. One standard method to reduce excess noise from initial molecular ion production is to normalize for the varying total HfF^+ number, which is measured simultaneously with Hf^+ number (see Methods). With ion number normalization (orange circles in Fig. 4), $(\sigma_{\varphi_u}^2 + \sigma_{\varphi_l}^2)^{1/2}$ still remains more than two times higher than the QPN limit due to excess noise from photodissociation.

Instead of monitoring and correcting for each source of technical noise, we use our simultaneous detection of both molecular orientations to normalize all common-mode noise in each experimental cycle. One might expect that a complete normalization of the differential spin polarization $\Delta\varphi$ requires simultaneous detection of all four states involved. However, simultaneously detecting two states (A and C or B and D) is adequate to remove most of the excess noise. Fluctuations in ion production, state preparation, and detection all give rise to excess noise that is positively cor-

related between N_A and N_C or between N_B and N_D . Furthermore, when the two spin precession fringes are in phase, common-mode phase fluctuations contribute to positive correlations between the same pairs of states. When the spin precession fringes are simultaneously near a zero-crossing we obtain the highest phase sensitivity. Positive correlations between pairs of these populations cancel excess noise resulting in a measurement of $\Delta\varphi$ at the QPN limit, represented by green squares in Fig. 4, both at early time and late time (~ 1.5 s).

When the spin precessions of the upper and lower doublets are out of phase the positive correlations from ion production, state preparation, and detection are still canceled at the zero-crossings. However, common-mode phase noise correlates negatively and cannot be eliminated simultaneously. This phase noise brings the scatter of $\Delta\varphi$ significantly higher than the QPN limit, as shown in Fig. 4 at $t \approx 742$ ms. In our experiment, the early time and late time in-phase measurements are for achieving a QPN-limited eEDM measurement, and the out-of-phase measurements allow us to characterize the phase noise.

In summary, we demonstrate a spin precession measurement at the quantum projection noise (QPN) limit with hundreds of ions and an interrogation time in excess of ~ 1.5 s. This is achieved by a combination of efficient quantum state preparation and orientation-selective photofragment imaging. This scheme will significantly increase the signal-to-noise ratio in the next generation of the eEDM measurement. Extending our state preparation to a larger number of scattered photons (~ 100), direct fluorescence imaging of a single molecular ion is within reach, even for molecules with unfavorable Franck-Condon factors and complex low-lying states, such as HfF^+ and ThF^+ .

Alternatively, with a colder sample of molecules, we may be able to resolve individual m_F states in photofragment imaging, opening the possibility to detection all four states simultaneously. By performing differential measurements on oriented polar molecules, one can extract clearer signals out of noisy background when testing fundamental symmetries⁴ or studying stereochemistry³⁷.

Methods

Experimental setup Both ThF^+ and HfF^+ experiments are performed in RF traps, which are described in Refs. [32, 36]. Both ThF^+ and HfF^+ ions are created by resonantly enhanced multiphoton ionization (REMPI) from neutral molecular beams of ThF and HfF, respectively. About 3000 ThF^+ ions and 20000 HfF^+ ions are trapped with ion cloud temperatures of about 10 K. Typical trap frequencies with 50 kHz RF trapping fields are 3 kHz in the X, Y directions, and 1 kHz in the Z direction. A rapidly rotating electric field (up to 350 kHz and 60 V/cm) is applied by adding sinusoidal voltages on the trap electrodes. Coils in an anti-Helmholtz configuration provide a linear magnetic field gradient at the center of the trap. An effective rotating magnetic field is generated by coupling ion circular micromotion to the magnetic field gradient, which is described in Ref. [30].

Orientation contrast The orientation contrast in Fig. 3(c) is defined by:

$$C_{-3/2} = \int_{y_c}^{+\infty} (I_{-3/2} - I_{+3/2}) dy \Big/ \int_{y_c}^{+\infty} (I_{-3/2} + I_{+3/2}) dy \quad (3)$$

$$C_{+3/2} = \int_{-\infty}^{y_c} (I_{+3/2} - I_{-3/2}) dy \Big/ \int_{-\infty}^{y_c} (I_{-3/2} + I_{+3/2}) dy \quad (4)$$

$$C = (C_{+3/2} + C_{-3/2})/2 \quad (5)$$

where $I_{\pm 3/2}$ and y_c are the 1D projected intensity and center line of the anisotropic photofragmentation, respectively.

Counting dissociated ions on gated imaging MCP with total ion number correction To reduce excess noise from ion detection we count the dissociated ions from an imaging MCP detector. By dispersing the dissociated ions onto the 40 mm imaging MCP detector, approximately 1000 ions can be counted with high fidelity. In addition, we develop a new method to extract the signal of the non-dissociated ions in the same cycle. The technical details of this method are described in Ref. [38]. Thus, we can use information of total ions to suppress the excess noise of ion creation. However, this method cannot reduce the technical noise of the photodissociation.

Fractional technical noises of ion creation and detection Both HfF^+ and ThF^+ ions are created in a two-step process. Firstly, hafnium or thorium plasma is generated by ablating the corresponding solid metal with a 5 ns, few mJ, 532 nm laser pulse from a Q-switched Nd:YAG laser. The hot plasma chemically reacts with SF_6 in buffer gas to create neutral HfF or ThF molecules in a supersonic beam. There is $\sim 20\%$ shot-to-shot fluctuation of molecular beam intensity, primarily coming from non-repeatable metal surface condition and ablation pulse energy fluctuation. Secondly, the neutral molecules in the beam are ionized by a two-photon resonantly enhanced multiphoton ionization (REMPI) process. Two tunable dye lasers pumped by one Nd:YAG laser generate these two photons. The REMPI adds an additional $\sim 20\%$ shot-to-shot fluctuation. In all, the number of trapped HfF^+ or ThF^+ has $\sim 30\%$ excess noise in our typical experiments. Similar to REMPI, two-photon resonance enhanced multiphoton dissociation (REMPD) for signal readout also requires tunable dye lasers. A $\sim 20\%$ shot-to-shot fluctuation is observed due to fluctuating pulse energies

and laser frequency.

Quantum projection noise limit

$$\sigma_{\Delta\phi}^2 = 2 \left(\frac{1}{N_t} \right) p_B (1 - p_B) + 2 \left(\frac{1}{N_t} \right) p_D (1 - p_D) \quad (6)$$

where N_t is the total number of detected dissociated ions in two adjacent cycles, and p_B and p_D are the probabilities of populations in the states B and D .

Reference.

1. DeMille, D. Quantum computation with trapped polar molecules. *Physical Review Letters* **88**, 067901 (2002).
2. Gorshkov, A. V. *et al.* Tunable superfluidity and quantum magnetism with ultracold polar molecules. *Physical Review Letters* **107**, 115301 (2011).
3. Bohn, J. L., Rey, A. M. & Ye, J. Cold molecules: Progress in quantum engineering of chemistry and quantum matter. *Science* **357**, 1002 (2017).
4. Safronova, M. S. *et al.* Search for new physics with atoms and molecules. *Reviews of Modern Physics* **90**, 25008 (2017).
5. Wolf, F. *et al.* Non-destructive state detection for quantum logic spectroscopy of molecular ions. *Nature* **530**, 457 (2016).
6. Chou, C. W. *et al.* Preparation and coherent manipulation of pure quantum states of a single molecular ion. *Nature* **545**, 203 (2017).

7. Ospelkaus, S. *et al.* Quantum-state controlled chemical reactions of ultracold potassium-rubidium molecules. *Science* **327**, 853 (2010).
8. Yan, B. *et al.* Observation of dipolar spin-exchange interactions with lattice-confined polar molecules. *Nature* **501**, 521 (2013).
9. Collopy, A. L. *et al.* 3D magneto-optical trap of yttrium monoxide. *Physical Review Letters* **121**, 213201 (2018).
10. Lien, C. Y. *et al.* Broadband optical cooling of molecular rotors from room temperature to the ground state. *Nature Communications* **5**, 4783 (2014).
11. Anderegg, L. *et al.* Laser cooling of optically trapped molecules. *Nature Physics* **14**, 890 (2018).
12. Truppe, S. *et al.* Molecules cooled below the Doppler limit. *Nature Physics* **13**, 1173 (2017).
13. Andreev, V. *et al.* Improved limit on the electric dipole moment of the electron. *Nature* **562**, 355 (2018).
14. Hudson, J. J. *et al.* Improved measurement of the shape of the electron. *Nature* **473**, 493 (2011).
15. De Marco, L. *et al.* A degenerate Fermi gas of polar molecules. *Science* **363**, 853 (2019).
16. Hudson, E. R. & Campbell, W. C. Dipolar quantum logic for freely rotating trapped molecular ions. *Physical Review A* **98**, 040302 (2018).

17. Ni, K. K., Rosenband, T. & Grimes, D. D. Dipolar exchange quantum logic gate with polar molecules. *Chemical Science* **9**, 6830 (2018).
18. Yu, P., Cheuk, L. W., Kozyryev, I. & Doyle, J. M. A scalable quantum computing platform using symmetric-top molecules. *arXiv:1905.06439* (2019).
19. Cairncross, W. B. *et al.* Precision measurement of the electron's electric dipole moment using trapped molecular ions. *Physical Review Letters* **119**, 153001 (2017).
20. Kozyryev, I. & Hutzler, N. R. Precision measurement of time-reversal symmetry violation with laser-cooled polyatomic molecules. *Physical Review Letters* **119**, 133002 (2017).
21. Flambaum, V. V., Demille, D. & Kozlov, M. G. Time-reversal symmetry violation in molecules induced by nuclear magnetic quadrupole moments. *Physical Review Letters* **113**, 103003 (2014).
22. Stadnik, Y. V., Dzuba, V. A. & Flambaum, V. V. Improved limits on Axionlike-particle-mediated P, T-violating interactions between electrons and nucleons from electric dipole moments of atoms and molecules. *Physical Review Letters* **120**, 13202 (2018).
23. Schneider, T., Roth, B., Duncker, H., Ernsting, I. & Schiller, S. All-optical preparation of molecular ions in the rovibrational ground state. *Nature Physics* **6**, 275 (2010).
24. Sta anum, P. F., Højbjerg, K., Skyt, P. S., Hansen, A. K. & Drewsen, M. Rotational laser cooling of vibrationally and translationally cold molecular ions. *Nature Physics* **6**, 271 (2010).

25. Schulte, M., Lörch, N., Leroux, I. D., Schmidt, P. O. & Hammerer, K. Quantum algorithmic readout in multi-ion clocks. *Physical Review Letters* **116**, 013002 (2016).
26. Glöckner, R., Prehn, A., Englert, B. G. U., Rempe, G. & Zeppenfeld, M. Rotational cooling of trapped polyatomic molecules. *Physical Review Letters* **115**, 233001 (2015).
27. Gresh, D. N., Cossel, K. C., Zhou, Y., Ye, J. & Cornell, E. A. Broadband velocity modulation spectroscopy of ThF^+ for use in a measurement of the electron electric dipole moment. *Journal of Molecular Spectroscopy* **319**, 1 (2016).
28. Zhou, Y. *et al.* Visible and ultraviolet laser spectroscopy of ThF. *Journal of Molecular Spectroscopy* **358**, 1 (2019).
29. Stuhl, B. K., Sawyer, B. C., Wang, D. & Ye, J. Magneto-optical trap for polar molecules. *Physical Review Letters* **101**, 243002 (2008).
30. Loh, H. *et al.* Precision spectroscopy of polarized molecules in an ion trap. *Science* **342**, 1220 (2013).
31. Ni, K.-K. *et al.* State-specific detection of trapped HfF^+ by photodissociation. *Journal of Molecular Spectroscopy* **300**, 12 (2014).
32. Ng, K. B. *et al.* Spectroscopy of the eEDM-sensitive state in ThF^+ . *In preparation* (2019).
33. McDonald, M. *et al.* Photodissociation of ultracold diatomic strontium molecules with quantum state control. *Nature* **535**, 122 (2016).

34. Beswick, J. A. & Zare, R. N. On the quantum and quasiclassical angular distributions of photofragments. *Journal of Chemical Physics* **129**, 164315 (2008).
35. Shagam, Y. *et al.* High efficiency state preparation and orientation-selective photodissociation of ThF⁺ and HfF⁺ for next generations of eEDM measurements. *In preparation* (2019).
36. Cairncross, W. B. *Searching for time-reversal symmetry violation with molecular ions: Quantum state control and photofragment imaging*. Ph.D. thesis, University of Colorado - Boulder (2019).
37. Heid, C. G., Walpole, V., Brouard, M., Jambrina, P. G. & Aoiz, F. J. Side-impact collisions of Ar with NO. *Nature Chemistry* **11**, 662 (2019).
38. Shagam, Y. *et al.* Simultaneous Image slicing and time of flight detection with an imaging MCP. *In preparation* (2019).

Competing Interests The authors declare that they have no competing financial interests.

Contributions All authors contributed to the work, including data collection, analysis, discussion, and writing of the manuscript.

Correspondence Correspondence and requests for materials should be addressed to Y. Zhou (email: yan.zhou@jila.colorado.edu) or Y. Shagam (email: yuval.shagam@jila.colorado.edu).

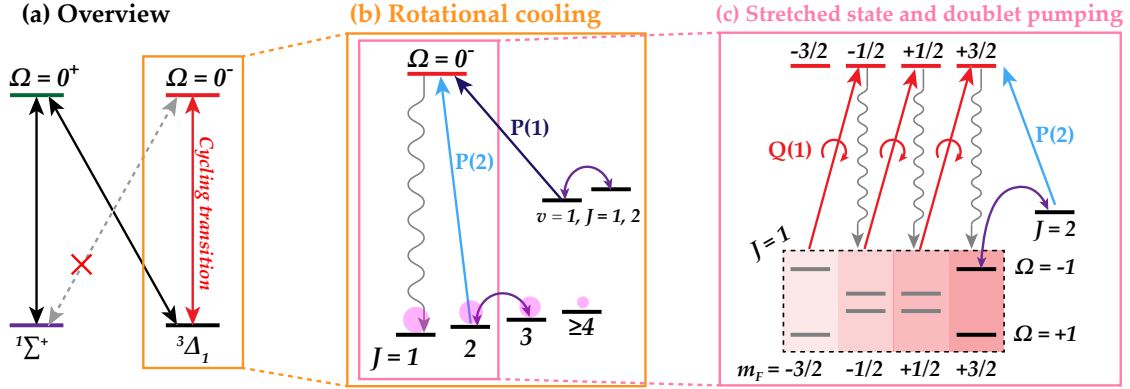


Figure 1: **Schematic diagram of single state preparation.** (a) An $\Omega = 0^+$ state bridges the low-lying $^1\Sigma^+$ and $^3\Delta_1$ states, while an $\Omega = 0^-$ state couples to $^3\Delta_1$ only. ThF^+ ions are created in $^3\Delta_1, v = 0$ directly, while HfF^+ ions are created in $^1\Sigma^+, v = 0$ and optically pumped to the $^3\Delta_1$ state via the $\Omega = 0^+$ state. (b) Using the $J = 2 \rightarrow J' = 1$ [$P(2)$] transition and mixing the $J = 2$ and $J = 3$ states via microwaves (purple curved arrows), the population is transferred to the target $J = 1$ state. Molecules that decay into excited vibrational states ($v = 1$) are recovered with their respective $J = 1 \rightarrow J' = 0$ [$P(1)$] repump (dark blue solid arrow), and the excited rotational states are mixed by microwaves. (c) Within the $J = 1$ state, the population is further pumped into the two fully stretched m_F states with circularly polarized light (red solid arrows). A single $|\Omega, m_F\rangle$ state can be selectively populated by coupling the other $|\Omega', m_F\rangle$ state to the $J = 2$ state with microwave, in which case it will be depleted and re-cycled.

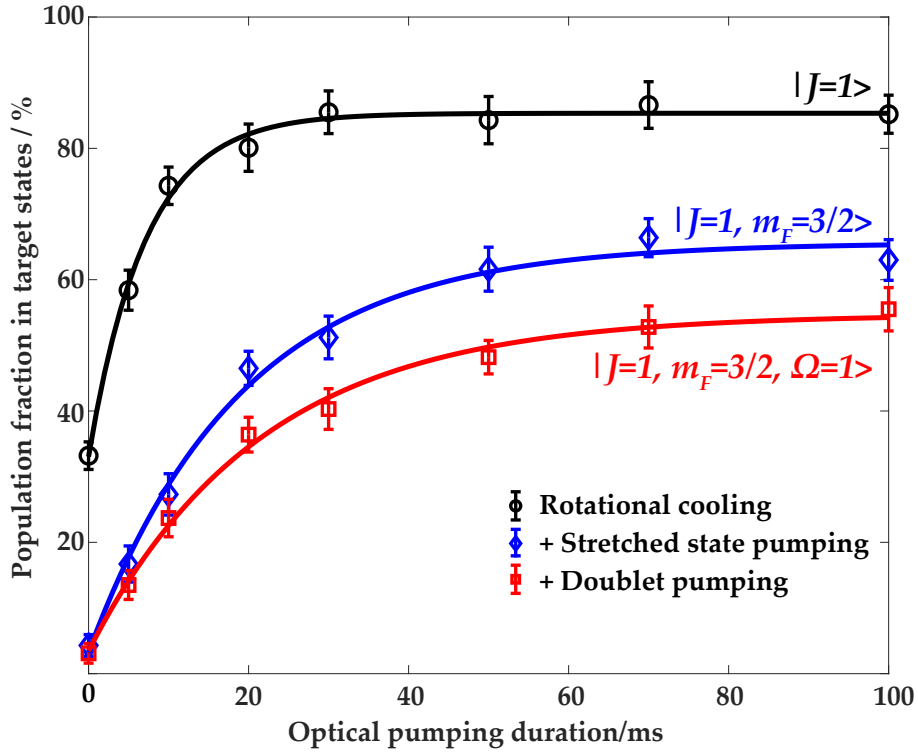


Figure 2: **Experimental demonstration of successively more elaborate quantum-state preparation of ThF^+ .** Rotational cooling concentrates 85% of the population in $J = 1$ in 20 ms. Including stretched state pumping, we prepare 60% of total ions into the two stretched states with $m_F = 3/2$ in 40 ms. Including doublet pumping, we move 50% of total population into one stretched state with a specific molecular orientation in 50 ms.

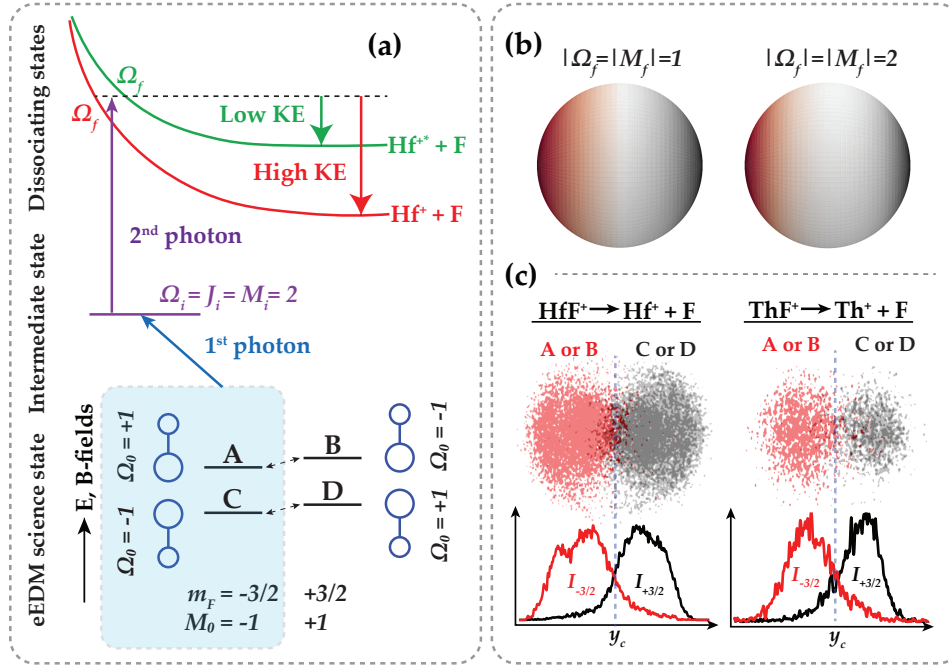


Figure 3: **Orientation-selective photofragmentation of HfF⁺/ThF⁺**. A schematic diagram of two-photon photodissociation of the eEDM sensitive, $^3\Delta_1$, $v = 0$, $J = 1$, $F = 3/2$ states, is shown in panel (a), where the product of M_0 and Ω_0 determines the molecular orientation. The first REMPDP photon excites the molecules to a bound intermediate state, $|\Omega_i = J_i = M_i = 2\rangle$, and the second REMPDP photon couples the intermediate state to the continuum states resulting in oriented photofragments, Hf⁺/Th⁺ and F atoms. The kinetic energy of fragments is determined by the energy in their internal states and the wavelength of the second REMPDP photon. Panel (b) shows theoretical angular distributions of the photofragments with different dissociating states³⁴. In panel (c), the Hf⁺/Th⁺ ions from each molecular orientation are mapped onto an imaging detector (2D plots), shown along with the resulting 1-D distributions. Their orientation contrasts (defined in Methods) are 78% and 67% respectively.

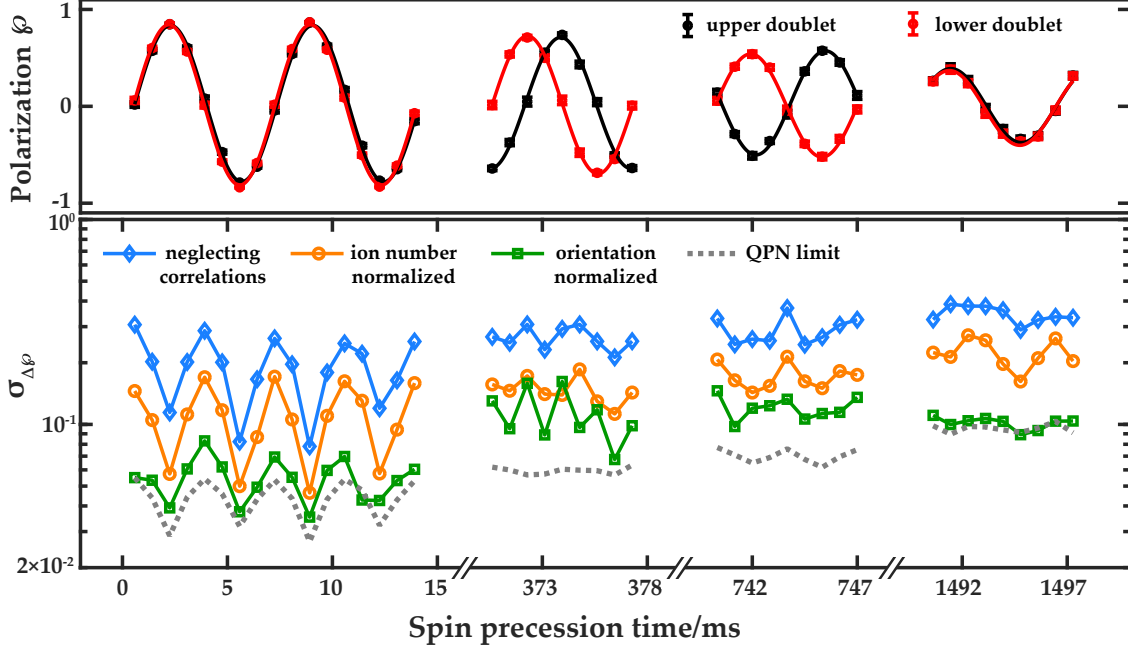


Figure 4: **Demonstration of a differential measurement at the quantum projection noise (QPN) limit.** The upper panel shows spin precessions of the upper and lower doublets, which are defined in the main text and have ~ 0.6 Hz frequency difference from different magnetic moments. The lower panel shows the scatter in $\Delta\phi$. From the scatter of ϕ_u and ϕ_l , determined independently, we would anticipate $\sigma_{\Delta\phi}$ (blue diamonds) to be 5 times larger than QPN limit (dotted line). With normalization by each cycle's ion production noise (orange circles), $\sigma_{\Delta\phi}$ is still more than two times the QPN limit. By extracting $\Delta\phi$ with simultaneous orientation-selective detection (green squares) we completely eliminate all common-mode noise to bring $\sigma_{\Delta\phi}$ close to the QPN limit when the fringes of the upper and lower doublets are in phase. Spin precession phase noise dominates the out-of-phase measurements (~ 745 ms). At early times (~ 5 ms), dips in $\sigma_{\Delta\phi}$ are observed at maximum or minimum polarizations (Eqn. (6)). The total signal ion numbers in two adjacent cycles (N_t in Eqn. (6)) of the four segmented measurements are 1400, 1000, 800, and 400, respectively. In this case, the coherence time of the spin precession fits to 1.8(1) s.